Biomaterials 201 (2019) 87–98

Contents lists available at ScienceDirect

Biomaterials

journal homepage: www.elsevier.com/locate/biomaterials

Nanoparticle-mediated intratumoral inhibition of miR-21 for improved survival in glioblastoma

Young-Eun Seo[a], Hee-Won Suh[a], Raman Bahal[b], Alexander Josowitz[a], Junwei Zhang[a], Eric Song[a], Jiajia Cui[a], Seth Noorbakhsh[c], Christopher Jackson[c], Tom Bu[a], Alexandra Piotrowski-Daspit[a], Ranjit Bindra[c], W. Mark Saltzman[a,*]

[a] Department of Biomedical Engineering, Yale University, New Haven, CT 06510, United States
[b] Department of Pharmaceutical Sciences, University of Connecticut, Storrs, CT 06269, United States
[c] Department of Therapeutic Radiology, Yale University School of Medicine, New Haven, CT, 06520, United States

ARTICLE INFO

Keywords:
Glioblastoma
Nanoparticles
MicroRNA
Convection-enhanced delivery

ABSTRACT

Glioblastoma (GBM) is the most common and deadly form of malignant brain tumor in the United States, and current therapies fail to provide significant improvement in survival. Local delivery of nanoparticles is a promising therapeutic strategy that bypasses the blood-brain barrier, minimizes systemic toxicity, and enhances intracranial drug distribution and retention. Here, we developed nanoparticles loaded with agents that inhibit miR-21, an oncogenic microRNA (miRNA) that is strongly overexpressed in GBM compared to normal brain tissue. We synthesized, engineered, and characterized two different delivery systems. One was designed around an *anti*-miR-21 composed of RNA and employed a cationic poly(amine-co-ester) (PACE). The other was designed around an *anti*-miR-21 composed of peptide nucleic acid (PNA) and employed a block copolymer of poly(lactic acid) and hyperbranched polyglycerol (PLA-HPG). We show that both nanoparticle products facilitate efficient intracellular delivery and miR-21 suppression that leads to PTEN upregulation and apoptosis of human GBM cells. Further, when administered by convection-enhanced delivery (CED) to animals with intracranial gliomas, they both induced significant miR-21 knockdown and provided chemosensitization, resulting in improved survival when combined with chemotherapy. The challenges involved in optimizing the two delivery systems differed, and despite offering distinct advantages and limitations, results showed significant therapeutic efficacy with both methods of treatment. This study demonstrates the feasibility and promise of local administration of miR-21 inhibiting nanoparticles as an adjuvant therapy for GBM.

1. Introduction

Glioblastoma (GBM) is the most common and aggressive malignant brain tumor among adults in the United States, with over 23,000 new cases diagnosed each year, resulting in over 14,000 deaths [1,2]. Despite medical advances, the prognosis for patients with GBM remains grim, with a median survival of 15 months after treatment and a five-year survival rate of a dismal 3.3% [3]. The current standard of care is surgical resection, followed by radiation and chemotherapy, usually with temozolomide (TMZ). However, these therapeutic interventions provide only a modest improvement in survival and result in nearly universal recurrence [4]. As our understanding of GBM continues to advance, it has become increasingly clear that treatments need to address the complexity and heterogeneity of the disease. Recently, alternate treatment approaches, such as microRNA-based therapeutics, have been introduced to target genetic and molecular alterations in GBM.

MicroRNAs (miRNAs) are small (20–22 nucleotide) non-coding RNAs that regulate gene expression by binding to and silencing complementary mRNA molecules. Because a single miRNA is responsible for the modulation of several targets, its effects extend to multiple genes and pathways. Importantly, miRNAs play a central role in various cellular processes that are altered in cancer, such as proliferation, migration and apoptosis. Out of over 200 miRNAs that are found to be dysregulated in GBM, miR-21 has been one of the most extensively studied and consistently reported to be overexpressed [5–7]. Through its regulation of PTEN, p53, TGF-β, MMP, and EGFR pathways, miR-21 plays a key role in GBM pathogenesis and progression [8–10]. As a promising therapeutic strategy, inhibition of miR-21 has been shown to disrupt the migratory ability of glioma cells, induce apoptosis and prevent tumor development [11–13]. Additionally, miR-21 suppression can

* Corresponding author.,
E-mail address: mark.saltzman@yale.edu (W.M. Saltzman).

https://doi.org/10.1016/j.biomaterials.2019.02.016
Received 19 December 2018; Received in revised form 10 February 2019; Accepted 14 February 2019
Available online 14 February 2019
0142-9612/

affect the sensitivity or resistance of GBM cells to other anticancer agents, including paclitaxel [14] and TMZ [15,16], and S-TRAIL [17]. Of course, the presence of the blood-brain barrier (BBB) prevents the transport of water-soluble agents, such as *anti*-miRs, into the brain, and even small amounts that might cross the BBB are subject to rapid clearance. Any effective strategy for getting miRs or *anti*-miRs into the brain would need to provide sufficient intratumoral drug levels that are sustained over a longer therapeutic window.

Local delivery strategies such as convection-enhanced delivery (CED) can facilitate intracranial distribution of therapeutic agents. CED features a slow and continuous infusion of therapeutic agents through catheters placed at the tumor site to achieve targeted and regional delivery over a controlled volume of tissue [18]. Although its safety and feasibility have been established in recent clinical trials [19], CED is generally a one-time event; therefore, CED of free miR or *anti*-miR in solution might not be sufficient to improve GBM treatment due to rapid clearance or degradation of most free drugs in the brain. To overcome these limitations, we propose to use polymeric nanoparticles (NPs) in combination with CED to achieve sustained and local delivery of agents that inhibit miR-21. In prior work, we have shown that this strategy is effective for sustained delivery of chemotherapy drugs [20–22] and radiosensitizers [23,24].

In this study, we developed two NP formulations designed for optimal delivery of two biochemically distinct miR-21 inhibitors. For gene delivery, a new class of cationic polymers called poly(amine-co-esters) (PACE) has been shown to provide excellent transfection efficiency with low toxicity, and is among the most effective non-viral gene delivery vectors reported in literature [25–28]. Here, we utilized PACE for the delivery of an antisense oligonucleotide against miR-21 (*anti*-miR-21). To achieve *in vivo* NP stability and improve intracranial distribution, we incorporated apolipoprotein E (ApoE) to the NP surface. Additionally, we optimized another approach for miRNA inhibition by utilizing antisense peptide nucleic acids (PNAs), which are designed to bind to complementary RNA with superior binding affinity and stability compared to other nucleic acid analogs. We encapsulated these miR-21 inhibiting PNAs in poly(lactic acid)-based NP formulations with different surface chemistries, which have been shown to influence cellular tropism and tumor uptake in the brain after CED [29]. We then compared the *in vitro* and *in vivo* transfection, intracranial distribution, and therapeutic efficacy of these NP formulations. Both systems achieved effective local delivery of two different miR-21 inhibitors, providing significant knockdown and survival benefit in rats with intracranial tumors. Our results highlight NP-mediated intratumoral miR-21 suppression as a promising strategy to improve GBM therapy.

2. Materials and methods

2.1. Materials

15-pentadecanolide (PDL, 98%), diethyl sebacate (DES, 98%) and *N*-methyldiethanolamine (MDEA, 99%), immobilized *Candida antarctica* lipase B (CALB) were purchased from Sigma-Aldrich. PNA monomers were purchased from ASM Research Chemicals. Poly(lactic acid) (Mw = 20.2 kDa, Mn = 12.4 kDa) was purchased from Lactel. Ethyl acetate (EtOAc), dimethylsulfoxide (DMSO), and acetonitrile (ACN) were obtained from J.T. Baker. Temozolomide was obtained from Enzo Life Sciences. RG2 rat glioma and U87 human glioblastoma cell lines were obtained from American Type Culture Collection (ATCC). Cells were grown in DMEM medium (Invitrogen) supplemented with 10% fetal bovine serum (Atlanta Biologicals) and 100 U/mL penicillin-streptomycin (Invitrogen) in a 37 °C incubator containing 5% CO_2.

2.2. Synthesis and characterization of nanoparticles

2.2.1. PACE-antimiR nanoparticles

The PACE polymers used in this study were synthesized through enzymatic copolymerization of PDL, DES, and MDEA using CALB as catalyst according to the procedures described previously [25]. This reaction was performed in two stages: oligomerization, carried out at 90 °C under 1 atm of argon gas, followed by polymerization under vacuum at 1.6 mmHg. The resulting polymers were analyzed by gel permeation chromatography (GPC) using a Waters HPLC system and compared to polystyrene standards to measure molecular weights. For all experiments, 10% PDL content polymers were used. Upon protonation at slightly acidic conditions (pH = 4.4–5.6), these PACE polymers are capable of condensing with RNA to form polyplexes. For all *in vitro* and *in vivo* studies, we used a chemically modified oligonucleotide mirVana miRNA Inhibitor (Thermo Fisher), designed specifically to inhibit miR-21, denoted *anti*-miR. NPs prepared with PACE and *anti*-miR at a weight ratio of 100:1 were used for all experiments. PACE polymer was dissolved in DMSO at a concentration of 100 mg/ml. For preparation of NPs for *in vitro* transfection, the polymer solution was first diluted in sodium acetate (NaAc) buffer (25 mM, pH = 5.2). After brief vortexing, the polymer solution was combined with the same volume of *anti*-miR solution (final concentration 100–500 nM) and vortexed for an additional 10 s. For cellular uptake, transfection and cell viability studies, NPs were incubated at room temperature for 10 min and then added to the cells.

2.2.2. Preparation of ApoE coated PACE-antimiR NPs for in vivo evaluation

NPs for *in vivo anti*-miR delivery were prepared immediately before CED. 1.6 μL polymer solution in DMSO (100 mg/ml) was diluted in 10.4 μL NaAc buffer (25 mM, pH = 4.8). After brief vortexing, the polymer solution was mixed with 5 μL water containing 2 μg *anti*-miR, followed by vortex for 10 s. NPs were incubated at room temperature for 10 min, followed by addition of 8 μL (10 mg/ml) ApoE (Abcam), and allowed to further incubate for 10 min. Equal volume of 60% trehalose was added and the resulting mixture was lyophilized. Immediately before CED, lyophilized NPs were resuspended in 25 μL NaAc buffer (25 mM, pH = 4.8). 20 μL of NP solution was infused into the rat caudate.

2.3. PNA PLA-HPG nanoparticles

All PNA oligomers were synthesized on solid support using standard Boc chemistry procedures [30]. The following PNA anti-21 sequence was used: TCAACATCAGTCTGATAAGCTA. Carboxytetramethylrhodamine (TAMRA, VWR) was conjugated to the N-terminus of PNAs with a hydrophilic bifunctional linker, Boc-miniPEG-3^{Tm} (Peptide International). PLA-HPG was synthesized as previously described [31]. To prepare PLA-HPG nanoparticles loaded with PNA, 50 mg of PLA-HPG was dissolved in 2.4 ml of EtOAc. Fifty nmol PNA was dissolved in 0.6 ml of DMSO. The PNA solution was then combined with the polymer solution resulting in a polymer/PNA solvent mixture. The resulting solution was added to 4 ml deionized (DI) water dropwise under vortex and sonicated with a probe sonicator (3 ×, 10s each). The emulsion was diluted in 10 ml of DI water and placed on a rotavapor for 20 min. The particle solution was washed by filtration using Amicon Ultra-15 centrifugal filter units (100 K MWCO) twice and resuspended in DI water. Resulting NPs were frozen and stored in −20 °C.

2.3.1. PNA PLA-HPG-CHO nanoparticles

To synthesize PLA-HPG-CHO NPs, PLA-HPG NPs (25 mg/ml) loaded with PNA were incubated with 0.1 M $NaIO_4$ (aq) and 10 × phosphate buffered saline (PBS) at 1:1:1 vol ratio for 20 min on ice. The reaction was quenched with 0.2 M Na_2SO_3 (aq) at 1:3 vol ratio and washed by filtration three times with DI water using Amicon Ultra-0.5 ml filters (100 K MWCO) and resuspended in DI water.

2.4. Nanoparticle characterization

2.4.1. Size and zeta potential measurements

The hydrodynamic diameter of freshly prepared NPs was measured by dynamic light scattering (DLS). NPs were diluted to 0.5 mg/ml and measured by dynamic light scattering (DLS) on a Malvern Nano-ZS (Malvern Analytical). For zeta potential measurements, 750 μL NPs at a concentration of 0.05 mg/ml in DI water were loaded into a disposable capillary cell and analyzed on a Malvern Nano-ZS. Transmission Electron Microscopy (TEM) was used to visualize particle morphology. 10 μL of the NP solution was placed on a CF400-CU TEM grid (Electron Microscopy Services) for 1 min. Grids were stained with a 0.2% uranyl acetate solution for 15 s and washed three times in DI water and then imaged on Tecnai Osiris TEM (FEI). For evaluation of particle stability, NPs were incubated in artificial cerebrospinal fluid (aCSF; Harvard Apparatus) at 37 °C and measured by DLS at designated time points using Malvern Nano-ZS.

2.4.2. Particle loading and in vitro release

20 μL PLA-HPG NPs were dissolved in 180 μL acetonitrile and incubated overnight. Absorbance at 260 nm was measured using a Nanodrop 8000 (Thermo Fisher). Release of PNAs from NPs was analyzed by incubating 5 mg NPs in 500 μL PBS at 37 °C under agitation. NPs were centrifuged using Amicon Ultra-0.5 ml filters (100 k MWCO) at designated time points and the filtrate was collected for analysis.

2.4.3. Evaluation of cellular uptake

To evaluate uptake of PACE-antimiR NPs, RG2 cells were plated in 24-well plates and treated with PACE NPs synthesized with FAM dye-labeled synthetic miRNA inhibitor (Thermo Fisher). Cells were washed three times with PBS and harvested at different time points (2 h, 4 h, 6 h). Flow cytometry was performed using Attune NxT (Invitrogen) and data analysis was performed using FlowJo 10.4.2 (FlowJo). For confocal microscopy, RG2 cells were plated on coverslips in 24-well plates and treated with fluorescently labeled PACE-antimiR NPs. After 6 h, NPs were removed, cells were washed three times with PBS, fixed in 4% paraformaldehyde for 15 min, and incubated in Alexa Fluor 647 phalloidin (Life Technologies) for 20 min as per manufacturer's instructions. Samples were mounted using VECTASHIELD HardSet Mounting Medium with DAPI (Vector Laboratories) and imaged on a Leica TCS SP5 confocal microscope (Leica). To evaluate uptake of PLA-HPG and PLA-HPG-CHO NPs, U87 cells were plated in 24-well plates and treated with NPs at 0.5 mg/ml. All PNA oligomers used in this study were labeled with TAMRA to enable fluorescent visualization. Cells were washed three times with PBS and harvested at different time points (4 h, 24 h). Flow cytometry was performed using BD LSR II (BD Biosciences) and data analysis was performed using FlowJo 10.4.2 (FlowJo). Confocal microscopy was performed as described above on U87 cells treated with NPs and stained with Alexa Fluor 488 phalloidin (Life Technologies).

2.4.4. In vitro transfection and reporter assay

For evaluation of miR-21 inhibition, U87 cells were seeded in 24-well plates at density of 50,000 cells/well in 500 μL media. Cells were transfected with a pMiR-21-5p Luciferase Reporter Vector (Signosis) using Lipofectamine 3000 (Invitrogen) according to the procedures provided by the manufacturer. 24 h after transfection, cells were harvested and transferred to a 96-well plate. Six hours later, cells were treated with PACE-antimiR-21 polyplexes at 100 nM and incubated for 48 h. Two days after transfection, the culture medium was removed and cells were lysed with 100 μL Reporter Lysis Buffer (Promega). After a freeze-thaw cycle, luciferase assay was performed on the cell lysates using the Luciferase Assay Reagent (Promega) according to the manufacturer's protocol. Additional 25 μL of cell lysate was used to quantify protein content using BCA protein assay kit (Pierce). Luciferase signal was divided by the amount of total protein content for comparison.

2.4.5. Quantification of miR-21 knockdown and PTEN upregulation by quantitative real-time PCR

The knockdown of miR-21 was determined by quantifying miR-21 levels from cell lysates after treatment with NPs. U87 cells were plated at a density of 200,000 cells/well in 24-well plates. Cells were treated with NPs or Lipofectamine at *anti*-miR concentration of 100 nM, or with buffer only as control. After 48 h of incubation, treatments were removed and total RNA was extracted from the cells using mirVana miRNA Isolation Kit (Thermo Fisher). cDNA synthesis was performed using TaqMan Advanced miRNA cDNA Synthesis Kit (Thermo Fisher). TaqMan Advanced miRNA Assays (Thermo Fisher). PCR reactions were prepared using TaqMan Fast Advanced Master Mix (Thermo Fisher), using probes against Taqman Advanced miRNA Assays for miR-21 and miR-26b (Thermo Fisher). For evaluation of PTEN expression, PCR reactions were prepared using PTEN and GAPDH TaqMan Gene Expression Assays (Thermo Fisher). The miRNA and PTEN levels were quantified using CFX Connect Real-Time PCR Detection System and CFX Manager Software (Bio-Rad). Relative expression was calculated using $2^{-\Delta\Delta Ct}$ and normalized to miR-26b and GAPDH, respectively.

2.4.6. Western blot analysis

U87 cells were seeded at a density of 200,000 cells/well in 24-well plates. 24 h after, cells were incubated with NPs or Lipofectamine at *anti*-miR concentration of 100 nM, or with buffer only as a control. After 48 h of incubation, treatments were removed and cells were lysed using RIPA Lysis and Extraction Buffer (Thermo Fisher) for Western blot analysis. The primary antibodies used were rabbit monoclonal to PTEN (Abcam) and rabbit polyclonal to β-Actin (Abcam).

2.4.7. Cell viability assays

U87 cells were plated in 96-well plates (5000 cells/well) and exposed to varying concentrations of NPs. After 48 h of incubation, NPs were removed and cell viability was evaluated using CellTiter-Glo Luminescent Cell Viability Assay (Promega). Luminescence was measured using a plate reader and cell viability was calculated as a percentage of untreated cells. For combination studies, cells were plated in 96-well plates (1000 cells/well) and exposed to varying concentrations of NPs. One day after, NPs were removed and TMZ was added to the wells (0–160 μM). After 6 days of incubation, treatments were removed and cell viability was measured as described above. For evaluation of synergy, U87 cells were treated as described above, fixed with paraformaldehyde and stained with Hoechst 33,342 nucleic acid stain (Thermo Fischer). Stained cells were imaged using Gen 5 Microplate Reader and Imager Software. Images were processed using CellProfiler and analyzed with Combenefit for evaluation of synergy as described previously [32]. Loewe additivity scores were used to assess synergistic combinations.

2.4.8. Annexin V assay

For the Annexin V apoptosis assay, PE Annexin V Apoptosis Detection Kit (BD Pharmingen) was used. Flow cytometry was performed using Attune NxT and data were analyzed using FlowJo 10.4.2 (FlowJo). PE-Annexin V positive and 7AAD-negative populations were identified as apoptotic cells.

2.4.9. Convection-enhanced delivery of NPs in the rat brain

All procedures involving animals were approved by the Yale University Institutional Animal Care and Use Committee (IACUC) and performed in accordance with the guidelines and policies of the Yale Animal Resource Center (YARC). Male Fischer 344 rats (Charles River Laboratories, 200–220 g) were used for distribution studies, and male RNU rats (Charles River Laboratories, 200–220 g) were used for evaluation of miR-21 knockdown and therapeutic efficacy. Animals were anesthetized using a mixture of ketamine (100 mg/kg) and xylazine (10 mg/kg), injected intraperitoneally. Anesthetized animals were then placed in a stereotaxic frame and prepped with alcohol and betadine. A

midline scalp incision was made to expose the coronal and sagittal sutures, and a burr hole was drilled 3 mm lateral to the sagittal suture and 0.5 mm anterior to the bregma in the right stratum. A 26G Hamilton syringe with a polyamide-tipped tubing was inserted into the burr hole at a depth of 5 mm from the surface of the brain and left to equilibrate for 5 min before infusion. Subsequently, 20 μL of NPs were infused at a rate of 0.667 μL/min. Once the infusion was finished, the syringe was left in place for another 7 min before removal of the syringe. Bone wax was used to fill the burr hole and skin was stapled and cleaned. After intramuscular administration of analgesic (Meloxicam, 1 mg/kg), animals were placed in a heated cage until full recovery.

2.4.10. Evaluation of NP distribution and retention in the healthy rat brain

To evaluate the volume of distribution, the brain was harvested immediately after NP infusion, flash frozen and sliced in 50 μm slices using a Leica Cryostat CM3000 (Leica). For retention studies, brains were harvested at various time points after infusion from 0 to 4 days, flash frozen and sliced. Slides were imaged using a Zeiss Lumar. V12 stereoscope (Carl Zeiss AG) and images were analyzed using a MATLAB code setting a threshold with Otsu's method.

2.4.11. Orthotopic tumor inoculation

Tumor inoculation was performed following the same surgical procedure as above. Instead of NPs, 5×10^5 U87 cells suspended in 3 μL PBS were injected over 3 min. For evaluation of *in vivo* transfection and distribution in the tumor-bearing brain, tumors were grown for 10 days before the administration of particles. For evaluation of therapeutic efficacy, tumors were grown for 7 days before the administration of particles.

2.4.12. Convection-enhanced delivery of NPs in the tumor bearing brain

CED in tumor-bearing rats was conducted following the exact same procedure as for the healthy rats, by reopening the burr hole used for tumor implantation. A micro-infusion pump (World Precision Instruments) was used to infuse 20 μL of NPs at a rate of 0.667 μL/min. The volume of distribution was determined using the same procedure as for the healthy brain.

2.4.13. Evaluation of in vivo miR-21 inhibition and apoptosis

For evaluation of *in vivo* miR-21 knockdown, animals were euthanized 48 h after CED and brains were harvested. The tumor tissue was separated from the adjacent normal brain regions from harvested rat brains. Total RNA was isolated from tumor tissue using miRVANA miRNA Isolation Kit (Ambion) according to manufacturer's instructions, and cDNA synthesis was performed using TaqMan Advanced miRNA cDNA Synthesis Kit (Thermo Fisher). PCR reactions were prepared using TaqMan Fast Advanced Master Mix (Thermo Fisher), using probes against Taqman Advanced miRNA Assays for miR-21 and miR-26b (Thermo Fisher). For evaluation of PTEN expression, PCR reactions were prepared using PTEN and GAPDH TaqMan Gene Expression Assays (Thermo Fisher). The miRNA and PTEN levels were quantified using CFX Connect Real-Time PCR Detection System and CFX Manager Software (Bio-Rad). Relative expression was calculated using $2^{-\Delta\Delta Ct}$ and normalized to miR-26b and GAPDH, respectively. To evaluate tumor apoptosis after CED, brains were harvested 48 h after CED and fixed in 4% paraformaldehyde for 24 h. TUNEL staining was performed by Yale Research Histology Services and imaged using an Axioimager A1 microscope and Axiocam mHRC color camera (Carl Zeiss).

2.4.14. Therapeutic efficacy study

Intracranial CED of NPs was performed 7 days after tumor implantation using the same procedure as for the evaluation of transfection. 24 h after CED, animals in the combination therapy group received a single intraperitoneal (IP) injection of TMZ (25 mg/kg) in PBS. Animals were monitored daily and euthanized when they showed clinical symptoms of tumor progression or greater than 15% loss in body weight, as deemed humanely necessary.

2.4.15. Statistical analysis

All studies were performed in triplicates and results are expressed as mean ± standard error. Statistical analysis was performed with Prism software (GraphPad) using Student's unpaired *t*-test or one-way ANOVA. P-values < 0.05 was considered statistically significant. All error bars represent standard error. Differences in survival curves were determined by Log-Rank test.

3. Results

We developed and characterized two alternate delivery systems for miR-21 inhibitors: PACE for delivery of RNA-based *anti*-miR-21 and surface-modified PLA for delivery of antisense PNA. The polymers were chosen based on their compatibility with the properties of each inhibitor, and we expected the resulting NPs to differ in their characteristics. PACE when combined with antimiR forms polyplexes, which rapidly dissociate in the cytosol after endocytosis, resulting in burst release of the antimiR. Thus, a major concern for the polyplex is stability. In contrast, PLA-HPG and PLA-HPG-CHO NPs, which are solid NPs, are expected to undergo slower degradation, resulting in a prolonged release of the encapsulated PNA. Our goal was to compare the advantages and disadvantages of the two formulations and evaluate their therapeutic potential in conjunction with CED. The experiments performed highlight the differences in their properties, leading up to the same end goal of achieving miR-21 suppression and survival benefit in an animal model.

3.1. Synthesis and characterization of PACE-antimiR nanoparticles

PACE polymers were synthesized through enzymatic copolymerization PDL, DES, and MDEA (Fig. 1a). PDL composition, calculated by dividing the moles of PDL by the moles of PDL plus DES, was 10%. PACE with 10% PDL content was chosen based on previous work, which demonstrated highly effective transfection of plasmid DNA [25]. The molecular weight of the resulting polymer was determined to be 10 kDa by GPC. Through nanocomplexation of the polymer with *anti*-miR-21 designed to inhibit miR-21, we formed PACE-antimiR NPs with uniform and spherical morphology as visualized by TEM (Fig. 1b). Using different buffer pH conditions during polyplex formation, we varied the size and surface charge of the resulting NPs. We observed that the pH of the sodium acetate buffer influenced the hydrodynamic diameter of NPs: decreasing the pH yielded smaller NPs (Fig. 1c). The zeta potential measurements were also highly dependent on the buffer pH such that the surface charge of NPs ranged from 33 mV to near neutral (Fig. 1d). When the NPs were suspended in artificial CSF (aCSF) to mimic the brain environment, the hydrodynamic diameters were larger and surface charges were close to neutral or slightly negative across the pH range (Fig. 1c and d).

3.2. Addition of ApoE improves in vivo stability

Untreated PACE-antimiR NPs aggregate when incubated in aCSF, reaching 600 nm in size within an hour (Fig. 1e). To improve stability of PACE-antimiR NPs for *in vivo* application, we explored various surface modifications. One approach is the incorporation of apolipoprotein E (ApoE), a blood plasma protein that mediates metabolism and transport of cholesterol as its physiological function. ApoE has previously been conjugated to NPs to enhance transport across the blood-brain barrier [33,34]. Additionally, ApoE functionalization has been shown to prolong brain retention and improve bioavailability of solid lipid NPs [35]. We found that an optimal weight ratio of PACE:antimiR:ApoE yielding the smallest particles was determined to be 100:1:50 (Fig. 1f). Further, we found that coating PACE-antimiR NPs with ApoE at this ratio prevents aggregation and that these NPs remained stable for over 48 h in

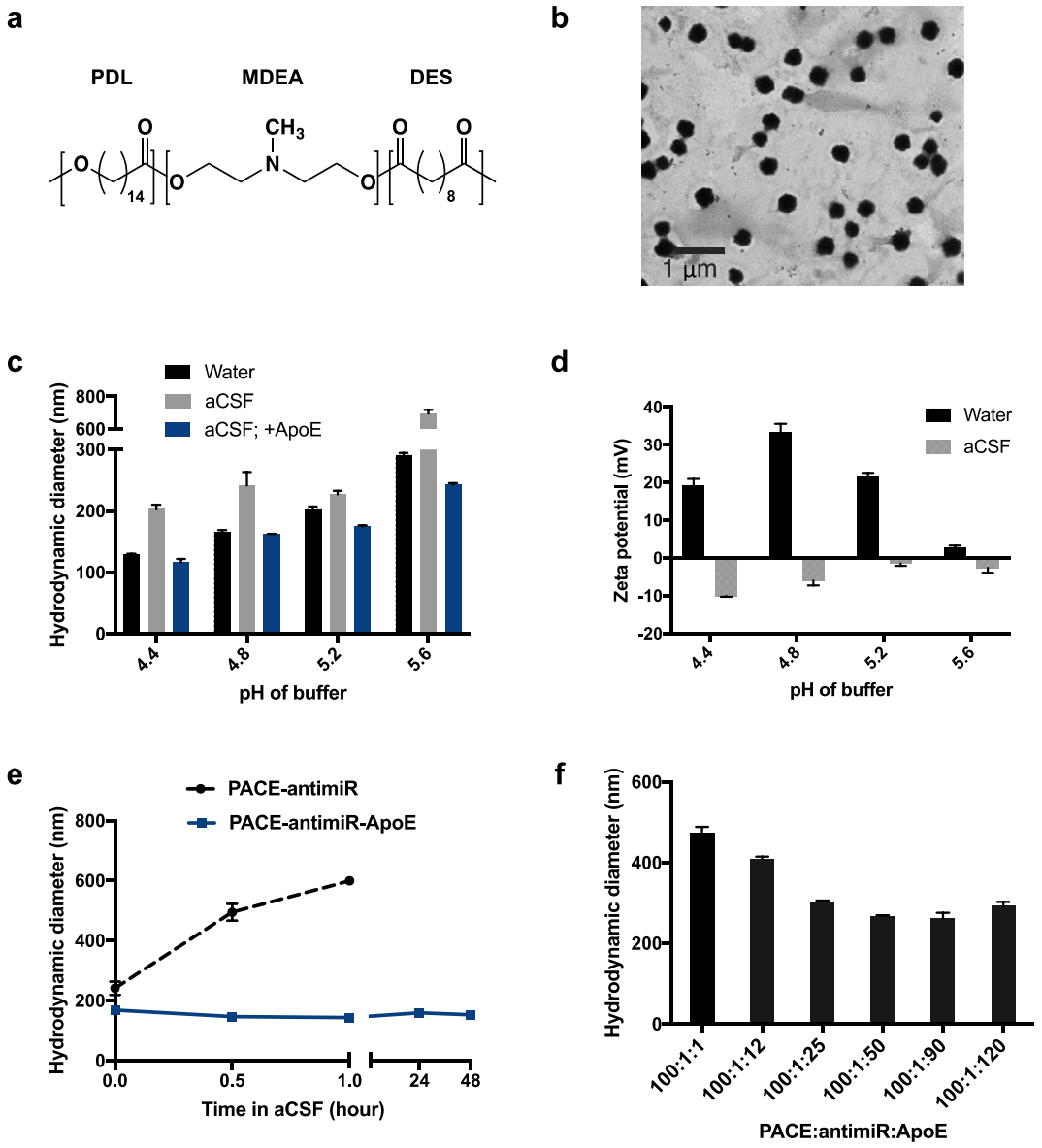

Fig. 1. Characterization of PACE nanoparticles. a. Chemical structure of PACE polymer. b. Visualization of PACE-antimiR NPs with TEM. c. Hydrodynamic diameters of NPs in water or aCSF under various buffer pH conditions. PACE-antimiR NPs coated with ApoE were also measured in aCSF. d. Zeta potential of NPs in water and aCSF under various buffer pH conditions. e. Addition of ApoE to PACE-antimiR NPs provides size stability in aCSF for at least 48 h. f. Hydrodynamic diameter of NPs with different weight ratios of PACE:antimiR:ApoE.

aCSF (Fig. 1e), making this an ideal formulation for *in vivo* delivery. Interestingly, the addition of ApoE reduced the effect of buffer pH on NP size; the range of hydrodynamic diameters in aCSF was narrower compared to those of uncoated NPs and remained smaller than 250 nm even at the highest buffer pH (Fig. 1c). To examine the distribution in the brain, we synthesized ApoE-coated and uncoated NPs with Cy3-labeled *anti*-miR and administered them by intracranial CED. We observed a significantly enhanced intracranial distribution with the addition of ApoE, resulting in a V_d of 13 mm^3, as compared to 2.3 mm^3 for uncoated NPs (Supplementary Fig. 1a). The luciferase expression in cells treated with PACE-antimiR-ApoE NPs was similar to that of uncoated NPs, confirming that the addition of ApoE does not interfere with transfection efficiency (Supplementary Fig. 1b).

3.3. Synthesis and characterization of PLA-HPG and PLA-HPG-CHO nanoparticles

PLA-HPG NPs encapsulating PNA *anti*-miRs were synthesized using a single emulsion solvent evaporation technique as previously described [31]. PLA-HPG-CHO NPs were prepared by conversion of PLA-HPG NPs with $NaIO_4$ treatment (Fig. 2a). TEM showed NPs of spherical morphology with the majority of particles between 100 and 150 nm in size as measured by dynamic light scattering (Fig. 2b). Analysis of NP size distribution using TEM, which enables visualization of the inner core, demonstrated a range of diameters between 20 and 100 nm (Supplementary Fig. 2a). The average hydrodynamic diameters of both formulations were less than 160 nm and zeta potentials were similar (Fig. 2c), indicating that the conversion does not affect the size or surface charge of the NPs. The average loading was determined to be 1.3 nmol PNA per 1 mg NP, which corresponds to a greater than 100% encapsulation efficiency after accounting for polymer loss during the fabrication process. Both NP formulations retained size stability in aCSF for at least 3 days (Fig. 2d). *In vitro* PNA release profiles showed that PLA-HPG-CHO NPs release PNA more slowly during the initial burst phase, with about 40% released after 24 h, compared to 50% for PLA-HPG NPs. After the first day, both formulations exhibited a slower

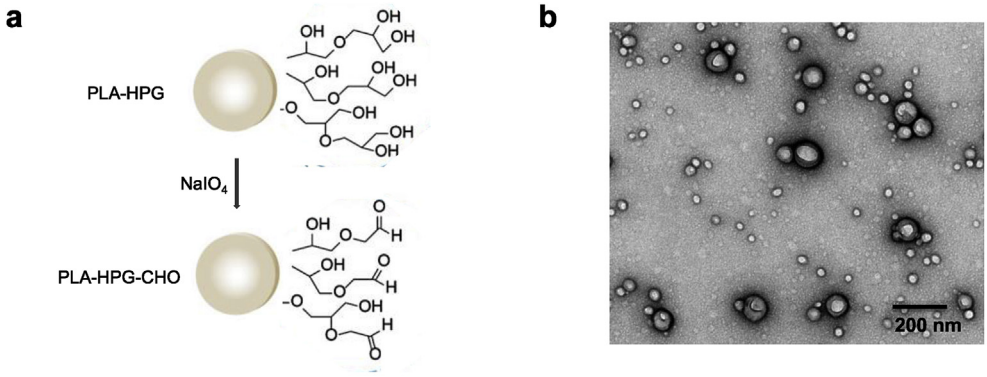

c

Formulation	Hydrodynamic diameter (nm)	Zeta potential (mV)	PNA loading (nmol/mg)
PLA-HPG	157 ± 5	-18	1.3 ± 0.3
PLA-HPG-CHO	153 ± 3	-22	1.3 ± 0.3

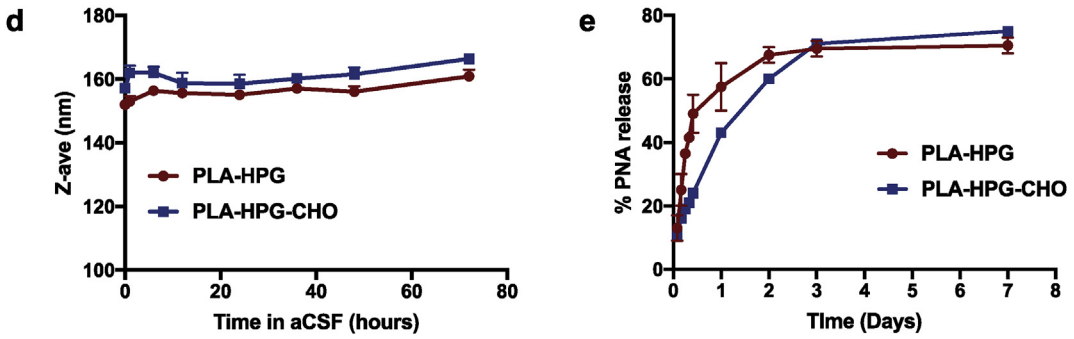

Fig. 2. Characterization of surface-modified PLA nanoparticles. a. A schematic of PLA-HPG to PLA-HPG-CHO conversion, b. TEM image of PLA-HPG NPs loaded with PNA c. Hydrodynamic diameter, zeta potential, and loading of PNA in PLA-HPG and PLA-HPG-CHO NPs. d. Size stability of NPs after incubation in aCSF. e. Release of PNA from NPs was measured over time and quantified as a percentage of amount loaded.

release for up to 3 days, after which the release rate was greatly reduced (Fig. 2e).

3.4. PACE-antimiR NPs show robust uptake in glioma cells

The major advantage of using PACE for *anti*-miR delivery is that we can achieve high transfection efficiency with minimal toxicity. When glioma cells were incubated with PACE-antimiR NPs, we detected internalization within 2 h of exposure, as measured by flow cytometry, with robust uptake observed between 4 and 6 h (Fig. 3b). Confocal microscopy confirmed internalization of FAM-labeled *anti*-miR in the perinuclear region delivered using PACE (Fig. 3a). In contrast, we did not observe any uptake in cells incubated with *anti*-miR alone (Fig. 3a), highlighting the utility and efficiency of PACE NPs for intracellular delivery.

3.5. PACE-antimiR NPs induce miR-21 knockdown, PTEN upregulation, and cell death

To monitor the inhibition of miR-21 we used a luciferase reporter system in which the target binding sequence for miR-21 was inserted into the 3′UTR of firefly luciferase. Endogenous miR-21 binds to the sequence, resulting in repression of luciferase gene expression, while the presence of *anti*-miR-21 can relieve this repression. Although *anti*-miR delivery can be achieved in cultured cells using conventional transfection reagents such as Lipofectamine, which has become a standard delivery approach for nucleic acids, its efficacy *in vivo* is greatly diminished due to its instability and toxicity. When incubated with U87 cells that have been transfected with the reporter vector, we observed an 8-fold increase in luciferase expression after treatment with PACE-antimiR NPs, corresponding to a much higher transfection compared to Lipofectamine-mediated delivery (Supplementary Fig. 1b). This was also confirmed with qRT-PCR, which demonstrated greater than 90% reduction in miR-21 expression, compared to ~50% reduction in cells transfected with Lipofectamine (Fig. 3c). Additionally, we performed a Western blot to measure the downstream effect of PACE-mediated miR-21 knockdown on expression of PTEN, a target protein of miR-21. Our analysis showed a 2–3 fold increase in PTEN levels in U87 cells treated with PACE-antimiR NPs (Fig. 3d and e). Furthermore, we observed dose-dependent cell death upon inhibition of miR-21, with

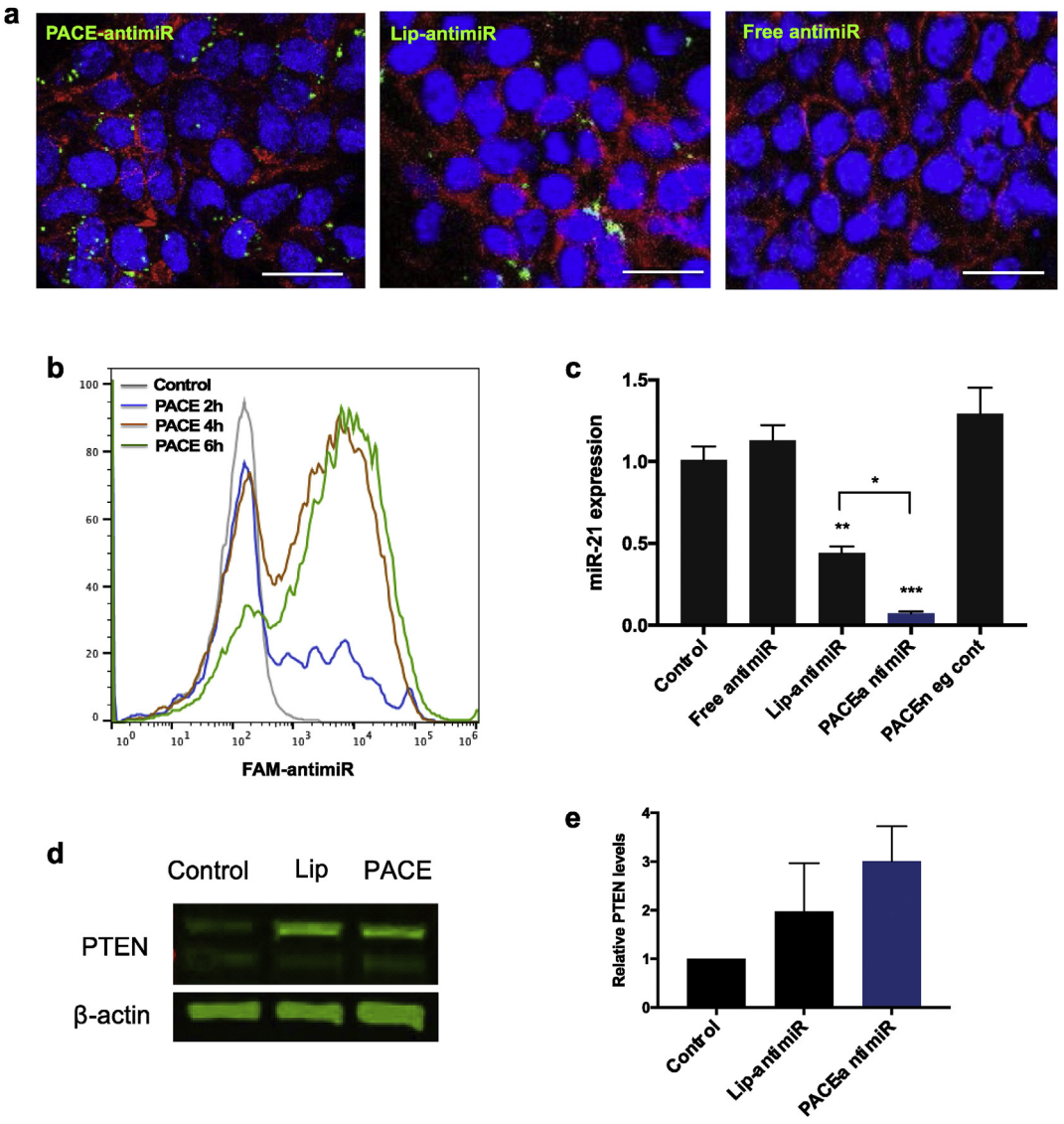

Fig. 3. Internalization and transfection of PACE NPs in glioma cells. a. Confocal microscopy shows internalization of PACE-antimiR NPs. Green = NPs. red = actin, blue = nuclei. Scale bar = 20 μm. b. Cellular uptake of PACE NPs was monitored overtime using flow cytometry. c. Knockdown of miR-21 after NP treatment was quantified by qRT-PCR. d. Western blot analysis of PTEN and beta actin levels in cells incubated with PACE-antimiR NPs or Lipofectamine. e. Western blot quantification showed elevated FTEN levels following NP treatment. (For interpretation of the references to color in this figure legend, the reader is referred to the Web version of this article.)

a marked decrease in cell viability around 500 nM *anti*-miR concentration (Supplementary Fig. 1c).

3.6. Surface properties influence cellular uptake of PLA-based NPs

Previous work has shown that surface properties of NPs influence cellular tropism and the rate of cellular uptake in the brain after CED [29]. Specifically, NPs decorated with 'stealth' surface coatings, such as HPG, facilitated intracranial distribution but reduced internalization, whereas NPs with 'bioadhesive' surface properties, such as HPG-CHO, exhibited preferential and enhanced uptake into tumor cells. Here, we observed that both PLA-HPG and PLA-HPG-CHO formulations facilitated uptake in U87 cells in as few as 4 h, though the total amount of internalization was low (Fig. 4a). Consistent with previous findings, tumor cell uptake was greater for PLA-HPG-CHO NPs than PLA-HPG NPs (Fig. 4b). Flow cytometry and confocal microscopy demonstrated much greater uptake of PLA-HPG-CHO NPs 24 h after particle administration.

3.7. PNA NPs provide miR-21 inhibition and PTEN upregulation

To evaluate the ability of antisense PNA NPs to inhibit miR-21, U87 cells were treated with either PLA-HPG or PLA-HPG-CHO NPs loaded with PNA. Analysis of miR-21 expression using qRT-PCR showed a 40% and 60% knockdown of miR-21 in cells treated with PLA-HPG and PLA-HPG-CHO NPs after 48 h of incubation with particles, respectively (Fig. 4c). We evaluated the effect of miR-21 suppression by measuring the levels of PTEN, a predicted target of miR-21 and a ubiquitous tumor suppressor that is inactive in many cancers [36]. Consistent with these findings, we observed a 2–3-fold increase in PTEN mRNA levels in U87 cells treated with either PLA-HPG or PLA-HPG-CHO NPs (Fig. 4d). Additionally, NP treatment induced dose-dependent glioma cell death, resulting in 30–40% reduction in cell viability at the highest treatment dose (Supplementary Fig. 2b).

3.8. Combination therapy with temozolomide enhances apoptosis

It has been reported that miR-21 promotes chemoresistance in GBM

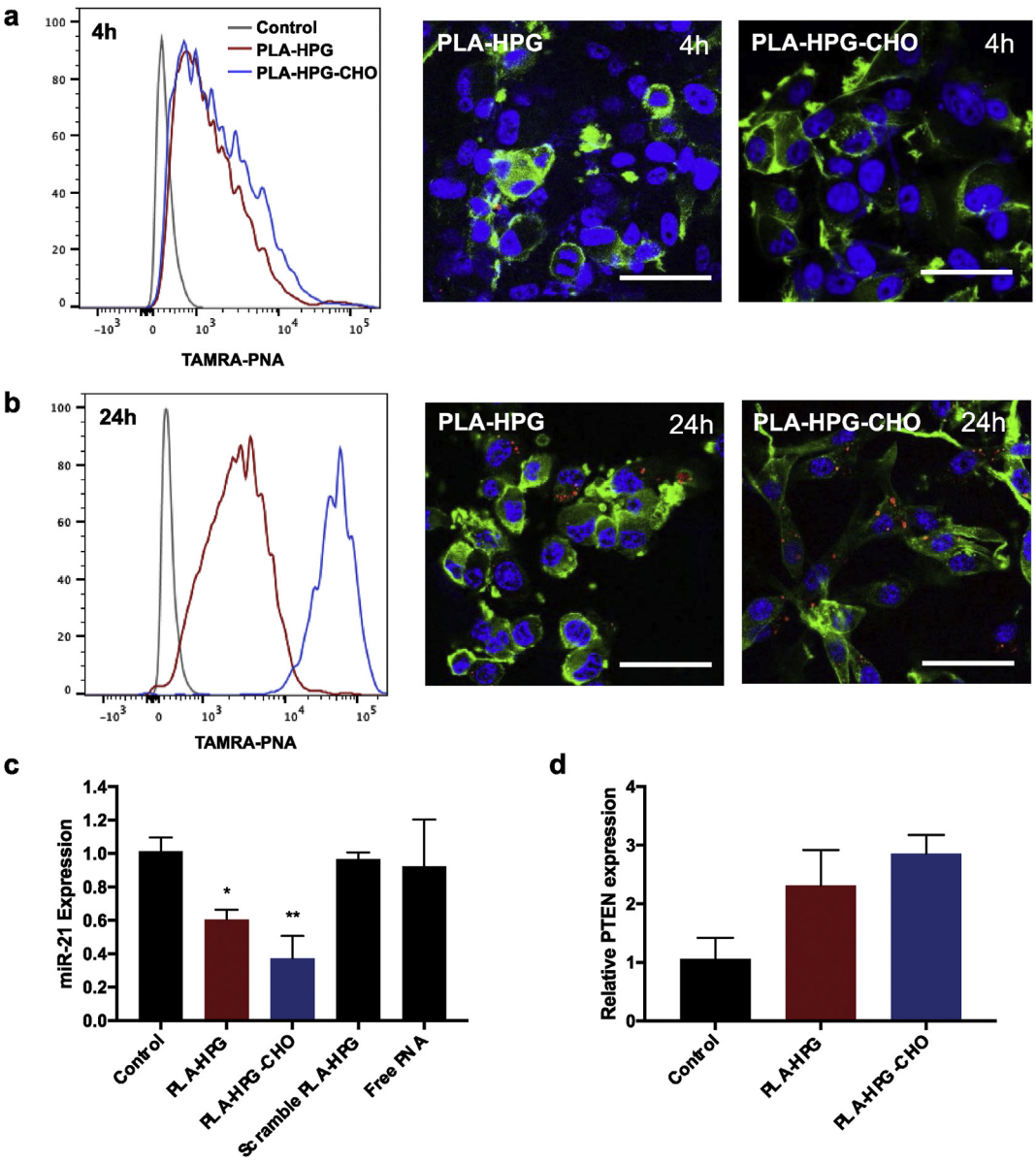

Fig. 4. Cellular uptake and transfection of PLA-HPG and PLA-HPG-CHO NPs. a Flow cytometry and confocal microscopy showed internalization of PNA in U87 cells after 4 h. red = NPs, green = actin, blue = nuclei. b. At 24 h. PLA-HPG-CHO NPs exhibit significantly higher uptake compared to PLA-HPG NPs. c. PNA NPs induce miR-21 knockdown in U87 cells after48 h of treatment. d. Inhibition of miR-21 results in PTEN upregulation in U87 cells. (For interpretation of the references to color in this figure legend, the reader is referred to the Web version of this article.)

and that miR-21 inhibition enhances the sensitivity of tumor cells to drugs such as TMZ [16]. Here, we tested the hypothesis that *anti*-miR-21 and TMZ could act synergistically to facilitate tumor cell death. Viability assays indicated that cells treated with PACE-antimiR or PLA-HPG-CHO NPs in addition to TMZ exhibited significantly reduced cell viability compared to the TMZ only group, resulting in an elevated response and higher sensitivity to TMZ treatment (Fig. 5a). To further validate these effects, we quantified apoptosis by performing PE-Annexin V and 7-AAD staining. The Annexin V-positive apoptotic population was significantly enhanced with co-treatment of PACE-antimiR NPs or PLA-HPG-CHO NPs with TMZ, with over 30% of Annexin V-positive cells in these cell populations compared to 7–15% observed in all other treatment groups (Fig. 5b, Supplementary Fig. 1d). The percentages of 7-AAD-positive cells were similar across all groups, suggesting that there were no significant effects on the late apoptotic cell population. The most dramatic increase in glioma cell death and apoptosis as a result of co-treatment was observed at higher TMZ concentrations (Fig. 5a, c), suggesting that a sufficient dose is required for the interaction to produce an enhanced response. We further assessed this potential for synergistic activity between NPs and TMZ using the Loewe additivity model. While combination of PLA-HPG NPs and TMZ had an additive effect on cell viability, combination of PLA-HPG-CHO NPs and TMZ demonstrated strong synergy at a lower range of treatment doses (Supplementary Fig. 2c). This sensitization effect supports the possibility of TMZ dose-reduction through co-treatment with miR-21-inhibiting NPs.

3.9. CED of NPs results in effective in vivo knockdown of miR-21

The intracranial distribution of NPs in tumor-bearing brains was assessed using dye-loaded NPs. Brains were harvested immediately after CED and representative coronal sections at the injection site were imaged (Fig. 6a). PLA-HPG and PLA-HPG-CHO NPs were found to have the large volumes of distribution, diffusing well beyond the injection

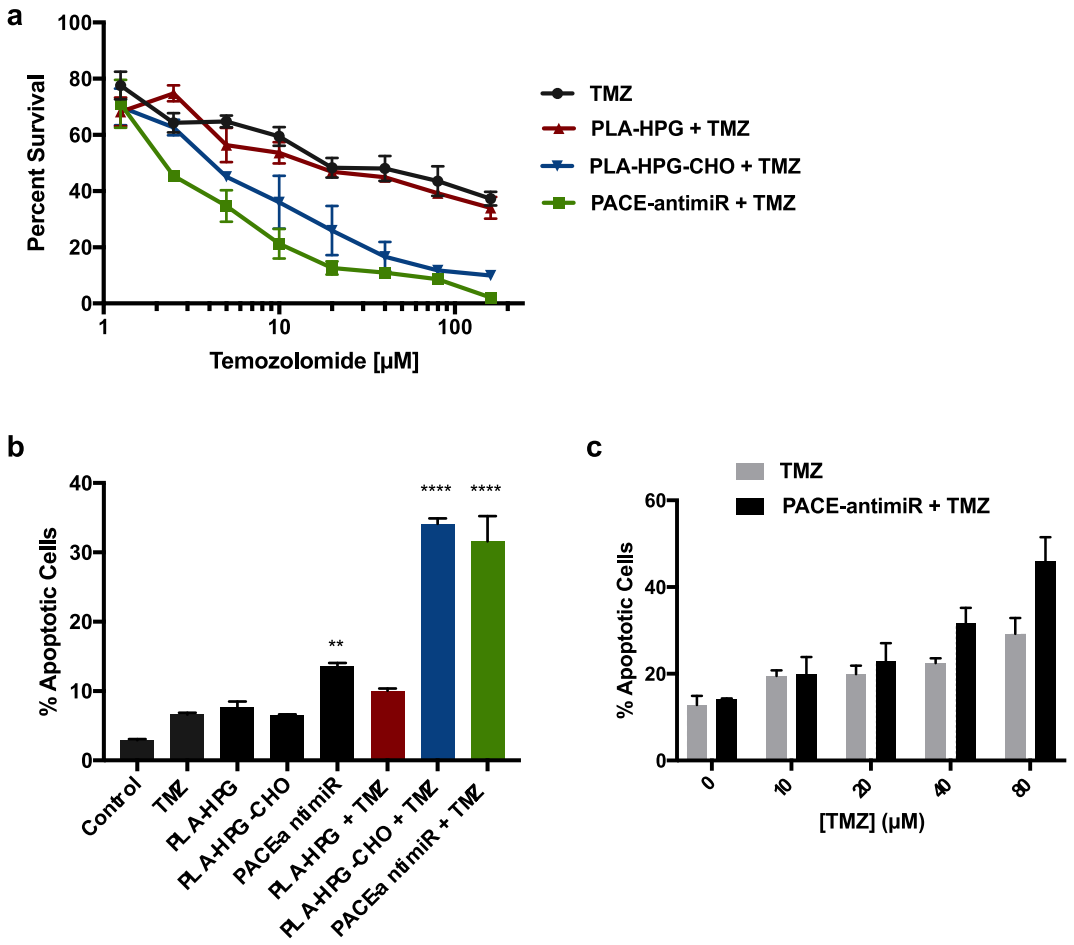

Fig. 5. Combined effects of NP-mediated miR-21 inhibition and TMZ on glioma cells. a Viability of U87 cells were quantified after treatment with varying doses of TMZ with or without miR-21 inhibiting NPs. b. Effects of miR-21 antagonism and TMZ on apoptosis were evaluated using Annexin V assay, c. Percentage of Annexin V-positive cells were quantified after incubation with NPs in combination with varying doses of TMZ. Chemosensitization effects of co-treatment were observed at higher TMZ concentrations.

site and covering most of the hemisphere. The distribution of PACE-antimiR NPs, even with the ApoE coating, was smaller compared to the other NP formulations. Next, we evaluated the ability of all NP formulations to inhibit miR-21 *in vivo*. U87 tumors were implanted in immunodeficient rats and grown for 10 days: this long duration between tumor implantation and CED ensured that tumors were large enough to be easily visualized and resected from the healthy brain tissue. PACE-antimiR-ApoE, PLA-HPG, or PLA-HPG-CHO NPs were administered by CED to the tumor site and the brains were harvested after 2 days (Fig. 6b). To assess relative miR-21 levels, tumors were homogenized and total RNA extracted. PCR analysis indicated that treatment with PACE-antimiR, PLA-HPG, or PLA-HPG-CHO NPs resulted in 67%, 53% and 49% knockdown of miR-21 expression compared to untreated animals (Fig. 6c). Additionally, consistent with our *in vitro* findings, we observed 1.8 and 3.4-fold increase in PTEN expression in tumors treated with PLA-HPG and PLA-HPG-CHO NPs, respectively (Supplementary Fig 2b). TUNEL stains of tumors showed an abundance of apoptotic cells in the NP treated animals, whereas no apoptotic nuclei were found in the control tumors (Fig. 6d).

3.10. Therapeutic efficacy studies

Finally, we tested whether miR-21 inhibiting NPs delivered by CED could provide therapeutic benefit *in vivo*. U87 intracranial tumors were established in immunodeficient rats and CED was performed 7 days after tumor implantation. We included combination therapy groups in which TMZ was administered by IP injection 1 day after NP infusion, following the *in vitro* treatment schedule (Fig. 7a). The median survival without treatment was 24 days (n = 7). In the groups treated with PACE-antimiR, PLA-HPG, and PLA-HPG-CHO NPs, median survival was extended to 28, 29, and 28 days, respectively (Supplementary Fig. 1e). Interestingly, 4 out of 16 (25%) of animals in the PNA NP treated groups were long-term survivors (≥60 days), whereas no animal in the control group survived past day 26. Administration of TMZ (25 mg/kg) conferred a statistically significant survival benefit (log-rank $p = 0.0005$), prolonging the median survival to 41 days (Fig. 7b). Combination treatment of PACE-antimiR NPs with TMZ further improved survival, resulting in a median survival of 50 days (log-rank $p = 0.0005$). This corresponds to a 108% increase in survival compared to PBS control and a 22% increase compared to the TMZ only group. The group treated with PLA-HPG-CHO NPs and TMZ also showed a significant response, with a median survival of 49 days (log-rank $p = 0.0001$) (Fig. 7c). PLA-HPG NPs in combination with TMZ did not confer a significant survival advantage over the control groups (Data not shown).

4. Discussion

Despite ongoing efforts towards the development of new therapies, GBM remains a devastating disease. Currently, there is no curative therapy, and overall survival has not changed significantly for the past 50 years. The standard of care, a multimodal approach of surgery, radiotherapy and chemotherapy, provides only a modest improvement in survival, and GBM tumors almost always recur after treatment. Drug

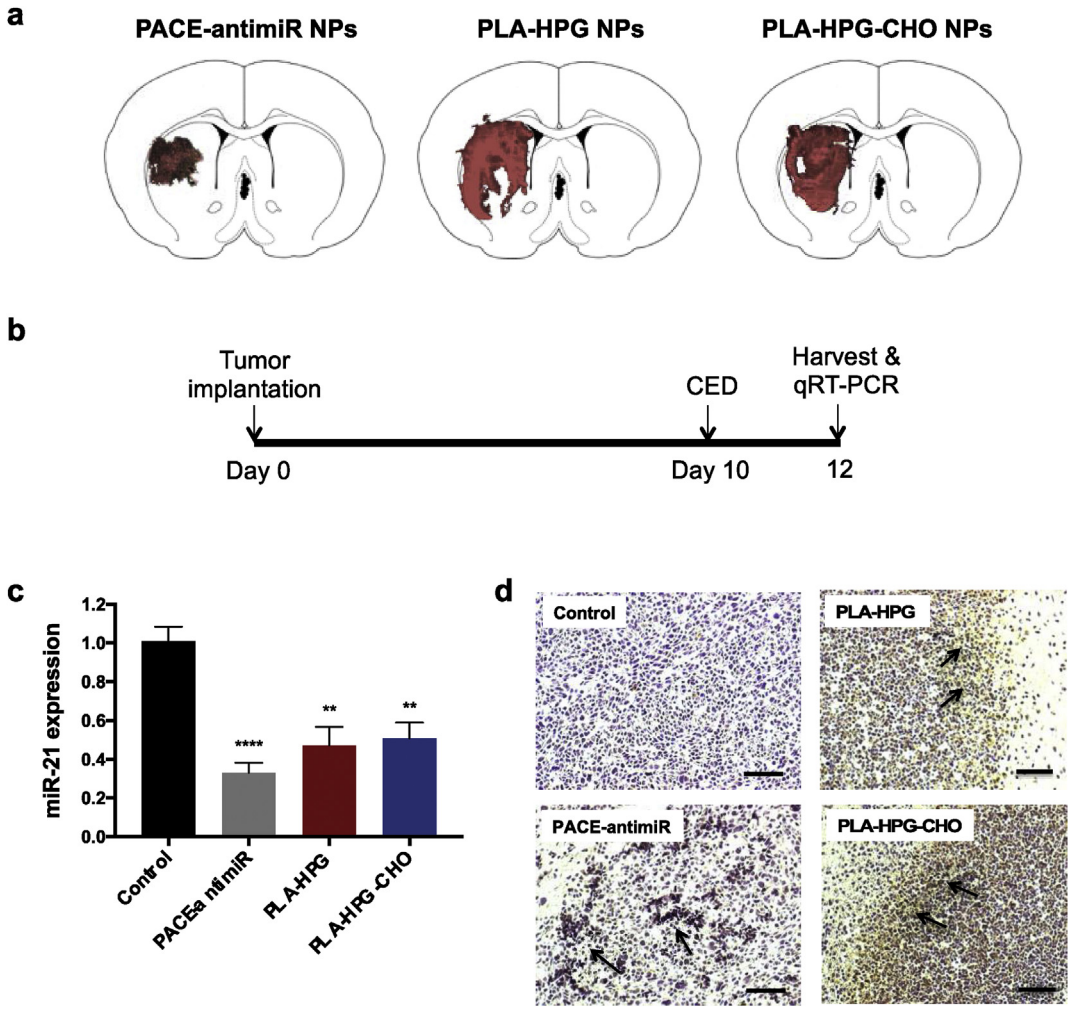

Fig. 6. CED of miR-21 inhibiting NPs in tumor-bearing brain. a. Intracranial distribution of fluorescently labeled NPs. Brains were harvested immediately after CED and 2D coronal sections were imaged. Representative sections at the injection site are shown. b. Schematic of treatment schedule for evaluation of miR-21 knockdown in intracranial U87 tumors. c. qRT-PCR analysis of miR-21 levels in tumors harvested 2 days after CED. d. TUNEL stain indicates presence of apoptotic cells (arrows) in tumors treated with NPs.

delivery across the BBB remains a paramount challenge, and achieving therapeutic intratumoral levels of agents is hindered by insufficient tumor uptake or rapid clearance from the brain environment. Local delivery strategies such as CED have been utilized to bypass the BBB and enhance intracranial distribution of these agents; in fact, there are at least 6 current clinical trials involving CED to treat brain tumors [37]. However, despite showing promising results in animal models and advancing to clinical trials, all of the completed trials with CED have failed to demonstrate therapeutic efficacy [19]. It is clear that CED is safe, and that it is an effective method for bypassing the BBB and allowing significant drug exposure to intracranial tumor cells. Therefore, the focus has shifted to the molecular mechanisms underlying GBM tumorigenesis and identifying better agents to deliver, based on our understanding of tumor biology. New approaches are aimed at utilizing their distinct molecular hallmarks, including miRNAs that are often deregulated in various cancers. We chose to target miR-21, one of the most extensively studied miRNAs in the context of cancer biology. Studies have shown that overexpression of miR-21 is a common feature of GBM tumors [6,11]. Numerous studies have highlighted the potential for miR-21 inhibition as a therapeutic approach, but currently available miRNA inhibitors require transfection methods that are not safe or feasible for use *in vivo*. Effective intracranial delivery of these agents, and achievement of high enough intratumoral levels for biological activity, is crucial to maximize their clinical efficacy.

Here, we developed two different approaches to deliver agents that can inhibit miR-21: 1) PACE for *anti*-miR delivery and 2) surface-modified PLA for PNA delivery. These polymers were chosen based on their compatibility with the material we sought to incorporate. In our previous work, we demonstrated that PACE can be used to enhance intracellular delivery of plasmid DNA, mRNA, and siRNA [25,27,38]. Building upon these past studies, we have now optimized a PACE formulation that can efficiently transfect *anti*-miR into glioma cells and identified conditions to produce small NPs that lead to high *in vitro* transfection efficiency. Addition of ApoE to the surface of these NPs provided stability and enhanced intracranial distribution after CED. For our alternate approach, we encapsulated charge-neutral antisense PNAs into PLA-HPG NPs, which degrade slowly and provide sustained release. The rate of tumor uptake can be enhanced with conversion to the bioadhesive form, PLA-HPG-CHO NPs, while maintaining their physiochemical properties that make them ideal for CED.

Even though our goal is to promote tumor cell death through miR-21 knockdown, the viability of healthy cells must be preserved. So far, most lipid or cationic polymer delivery vectors have not been suitable for *in vivo* applications due to their low transfection efficiencies and toxicity issues [39,40]. Using our NP formulation, we have been able to achieve up to 90% inhibition of miR-21 *in vitro* at a greater efficiency than a standard delivery approach using Lipofectamine. To evaluate the downstream effects of miR-21 inhibition, PTEN levels were quantified

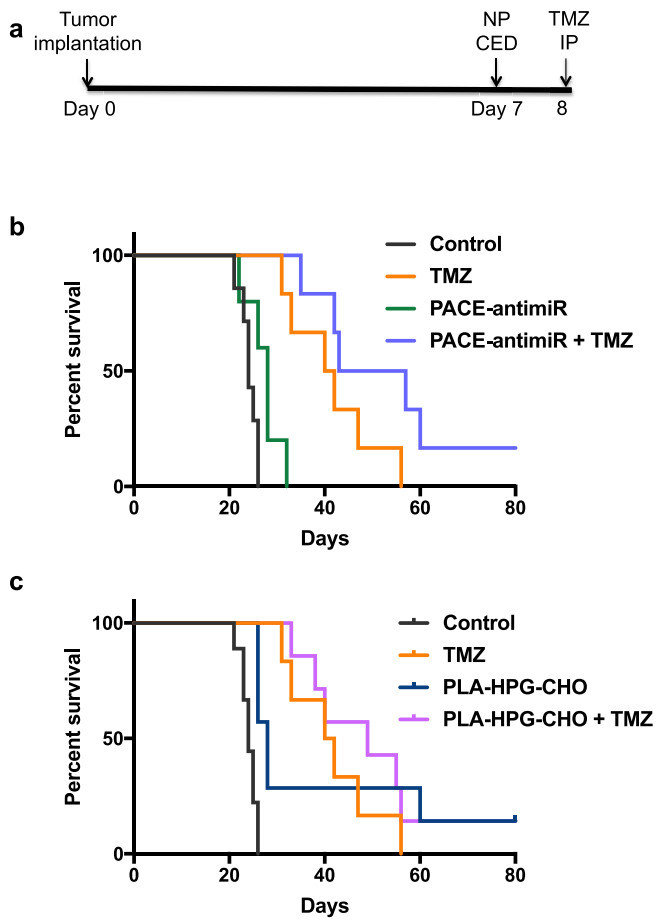

Fig. 7. Therapeutic efficacy study using U87 glioma model in RNU immunodeficient rats. a Schematic of treatment schedule. CED was performed 7 days after tumor implantation. Animals in combination therapy group received TMZ 24 h after CED. b. Kaplan-meier survival curve comparing groups treated with PACE-antimiR NPs alone or in combination wtih TMZ. c. Co-treatment of PLA- HPG-CHO NPs and TMZ conferred a significant survival benefit over the control groups.

after NP treatment. Because PTEN is a direct target of miR-21 and their expressions are negatively correlated, we predicted that miR-21 suppression would result in increased PTEN expression [10]. It is important to note that about 70% of GBMs are characterized by loss of PTEN [2], and this aberrant expression is associated with a malignant phenotype and poor patient survival [41]. As expected, NP-mediated miR-21 inhibition resulted in increased expression of PTEN. Additionally, these cells exhibited dose-dependent cell death, suggesting that PTEN upregulation may be a mechanism of this functional effect. These observations are consistent with previous findings and imply that miR-21 dependent modulation of PTEN may have biological relevance in cell proliferation and tumor growth. Although we can achieve effective inhibition of miR-21 and PTEN upregulation, our data indicated that a high *anti*-miR dose is required to have a significant inhibitory effect (IC50 ~ 500 nM). Because miR-21 regulates the expression of many different mRNAs, it is unlikely that the functional effect of its inhibition (i.e. cell death) is due to a single target. Our results suggest that there are likely other mechanisms that promote tumor cell survival and that miR-21 suppression alone may not be sufficient to attain therapeutic benefit.

To improve survival in animals with intracranial tumors, we tested combination therapy with TMZ, based on the evidence that miR-21 inhibition enhances the chemosensitivity of glioma cells [16,42]. When cells were pre-treated with NPs, we observed significant growth inhibition and a reduced IC50 for TMZ. Additionally, our results from Annexin V assays showed the highest percentage of apoptotic populations in cells treated with both NPs and TMZ. Interestingly, co-treatment of PLA-HPG-CHO NPs and TMZ induced the most dramatic increase in apoptosis, likely as a result of the high rate of tumor uptake of PLA-HPG-CHO particles compared to the other formulations. Our data, together with previous findings, imply that NP-mediated miR-21 knockdown may reduce TMZ resistance by priming tumor cells to undergo apoptosis and suppressing their proliferative capacity. From these results, we suggest that miR-21 suppression prior to chemotherapy may be a promising approach to enable dose reduction and minimize systemic toxicity.

The addition of ApoE to PACE-antimiR NP provided size stability, improved intracranial distribution, and facilitated tumor penetration when administered by CED. We chose this approach based on previous studies demonstrating that the addition of ApoE to the NP surface aids in drug delivery across the BBB by facilitating interaction of these NPs with brain endothelial cells [33,34]. This strategy has been employed to aid in delivery of drugs such as loperamide that normally have poor brain entry after systemic administration [43]. Because the *in vivo* environment is highly dynamic and the outcome is often difficult to predict based on *in vitro* results, our approach was to evaluate and compare multiple promising NP formulations in animal models. We formed our rationale based on the strengths of each formulation. We predicted that the sustained release properties of the PLA-HPG and PLA-HPG-CHO NPs would be beneficial to achieve prolonged therapeutic effects of PNA-induced miR-21 knockdown. In contrast to this prolonged release pattern, PACE-antimiR NPs likely exhibit a rapid dissociation with *anti*-miR upon endocytosis in the acidic environment. Consistent with our previous findings, we observed heterogeneous and non-uniform distribution of NPs in tumor-bearing brains [44]. We expect that the presence of the tumor affects NP distribution patterns, but that the overall volumes of distribution (V_d) would not vary significantly compared to those observed in healthy brains. Although the V_d of PACE-antimiR-ApoE NPs is smaller compared to the V_d that can be achieved with other polymeric NPs, we hypothesized that their high transfection efficiency may compensate for these limitations. Furthermore, the observed distribution for each of the three NP formulations was more than sufficient for coverage of a typical orthotopic tumor using this model. We believe that the both sustained release and enhanced intracranial retention are key components to achieve therapeutic effect.

CED of NPs in animals with intracranial gliomas resulted in significant reduction in intratumoral miR-21 expression compared to those of untreated animals. Additionally, histological analysis revealed presence of apoptotic cells in these tumors. These findings were extended to therapeutic efficacy studies in which we measured median survival of tumor-bearing animals after treatment with NPs alone or in combination with TMZ. Although treatment with any of the NP formulations alone did not confer a survival benefit, co-treatment with TMZ provided a significant therapeutic effect, producing markedly longer survival times. Our studies showed a 104% and a 108% increase in median survival using combinations of TMZ with PLA-HPG-CHO NPs and PACE-antimiR NPs, respectively. These results are consistent with the dramatic increase in apoptosis and cell death observed *in vitro*, and may be attributed to the effective transfection provided by PACE-antimiR NPs, and preferential uptake observed with PLA-HPG-CHO NPs into tumor cells [29].

5. Conclusions

In summary, we highlight a new approach for local therapy of GBM utilizing NPs as a delivery platform for two types of miR-21 inhibitors. These NPs enable efficient intracellular delivery, resulting in miR-21 suppression, upregulation of its target protein, tumor growth inhibition and apoptosis in combination with TMZ. CED of NPs facilitated intracranial distribution, retention, and miR-21 knockdown *in vivo*. Further, our approach of combination therapy demonstrated

therapeutic efficacy, prolonging survival of animals with intracranial tumors. Additional research is needed to determine the mechanism of synergy between miR-21 inhibitors and TMZ, which could help develop a more optimal, clinically relevant dosing schedule. Although no systemic or neurological toxicity was observed in our studies, the possibility of off-target effects should be considered. Overall, our results provide motivation for further development of NP-mediated miR-21 knockdown as a therapeutic approach to treat GBM.

Acknowledgements

This work was supported by the National Institutes of Health (R01 CA149128). A.S.P. was supported in part by NIH NRSA T32 (T32GM86287) and F32 (F32HL142144) Postdoctoral Fellowships.

Appendix A. Supplementary data

Supplementary data to this article can be found online at https://doi.org/10.1016/j.biomaterials.2019.02.016.

References

[1] M.L. Bondy, et al., Brain tumor epidemiology: concensus from the brain tumor epidemiology consortium (BTEC), Cancer 113 (7 Suppl) (2008) 1953–1968.
[2] H. Ohgaki, P. Kleihues, Epidemiology and etiology of gliomas, Acta Neuropathol. 109 (1) (2005) 93–108.
[3] Central Brain Tumor Registry of the United States, http://www.cbtrus.org/factsheet/factsheet.html, accessed 12 June, 2015..
[4] S. Sathornsumetee, J.N. Rich, New treatment strategies for malignant gliomas, Expert Rev. Anticancer Ther. 6 (7) (2006) 1087–1104.
[5] H.G. Moller, et al., A systematic review of microRNA in glioblastoma multiforme: micro-modulators in the mesenchymal mode of migration and invasion, Mol. Neurobiol. 47 (1) (2013) 131–144.
[6] M. Piwecka, et al., Comprehensive analysis of microRNA expression profile in malignant glioma tissues, Mol Oncol 9 (7) (2015) 1324–1340.
[7] S.A. Ciafrè, et al., Extensive modulation of a set of microRNAs in primary glioblastoma, Biochem. Biophys. Res. Commun. 334 (4) (2005) 1351–1358.
[8] T. Papagiannakopoulos, A. Shapiro, K.S. Kosik, MicroRNA-21 targets a network of key tumor-suppressive pathways in glioblastoma cells, Cancer Res. 68 (19) (2008) 8164–8172.
[9] G. Gabriely, et al., MicroRNA 21 promotes glioma invasion by targeting matrix metalloproteinase regulators, Mol. Cell Biol. 28 (17) (2008) 5369–5380.
[10] X. Zhou, et al., Downregulation of miR-21 inhibits EGFR pathway and suppresses the growth of human glioblastoma cells independent of PTEN status, Lab. Invest. 90 (2) (2010) 144–155.
[11] J.A. Chan, A.M. Krichevsky, K.S. Kosik, MicroRNA-21 is an antiapoptotic factor in human glioblastoma cells, Cancer Res. 65 (14) (2005) 6029–6033.
[12] Y. Li, et al., A miR-21 inhibitor enhances apoptosis and reduces G(2)-M accumulation induced by ionizing radiation in human glioblastoma U251 cells, Brain Tumor Pathol. 28 (3) (2011) 209–214.
[13] X. Zhou, et al., Reduction of miR-21 induces glioma cell apoptosis via activating caspase 9 and 3, Oncol. Rep. 24 (1) (2010) 195–201.
[14] Y. Ren, et al., MicroRNA-21 inhibitor sensitizes human glioblastoma cells U251 (PTEN-mutant) and LN229 (PTEN-wild type) to taxol, BMC Canc. 10 (2010) 27.
[15] L. Shi, et al., MiR-21 protected human glioblastoma U87MG cells from chemotherapeutic drug temozolomide induced apoptosis by decreasing Bax/Bcl-2 ratio and caspase-3 activity, Brain Res. 1352 (2010) 255–264.
[16] X. Qian, et al., Sequence-dependent synergistic inhibition of human glioma cell lines by combined temozolomide and miR-21 inhibitor gene therapy, Mol. Pharm. 9 (9) (2012) 2636–2645.
[17] M.F. Corsten, et al., MicroRNA-21 knockdown disrupts glioma growth in vivo and displays synergistic cytotoxicity with neural precursor cell delivered S-TRAIL in human gliomas, Cancer Res. 67 (19) (2007) 8994–9000.
[18] R.H. Bobo, et al., Convection-enhanced delivery of macromolecules in the brain, Proc. Natl. Acad. Sci. Unit. States Am. 91 (1994) 2076–2080.
[19] S. Kunwar, et al., Phase III randomized trial of CED of IL13-PE38QQR vs Gliadel wafers for recurrent glioblastoma, Neuro Oncol. 12 (8) (2010) 871–881.
[20] A.J. Sawyer, et al., Convection-enhanced delivery of camptothecin-loaded polymer nanoparticles for treatment of intracranial tumors, Drug Delivery. Translational Res. 1 (2011) 34–42.
[21] A. Gaudin, et al., PEGylated squalenoyl-gemcitabine nanoparticles for the treatment of glioblastoma, Biomaterials 105 (2016) 136–144.
[22] J. Zhou, et al., Highly penetrative, drug-loaded nanocarriers improve treatment of glioblastoma, Proc. Natl. Acad. Sci. U.S.A. 110 (29) (2013) 11751–11756.
[23] A.R. King, et al., Local DNA repair inhibition for sustained radiosensitization of high grade gliomas, Mol. Canc. Therapeut. 16 (8) (2017) 1456–1469.
[24] E.M. Chen, et al., Biodegradable PEG-poly(ω-pentadecalactone-co-p-dioxanone) nanoparticles for enhanced and sustained drug delivery to treat brain tumors, Biomaterials 178 (2018) 193–203.
[25] J. Zhou, et al., Biodegradable poly(amine-co-ester) terpolymers for targeted gene delivery, Nat. Mater. 11 (1) (2011) 82–90.
[26] J. Cui, et al., Ex vivo pretreatment of human vessels with siRNA nanoparticles provides protein silencing in endothelial cells, Nat. Commun. 8 (1) (2017) 191.
[27] Y. Jiang, et al., A “top-down” approach to actuate poly(amine-co-ester) terpolymers for potent and safe mRNA delivery, Biomaterials 176 (2018) 122–130 1878-5905 (Electronic).
[28] A.C. Kauffman, et al., Tunability of biodegradable poly(amine-co-ester) polymers for customized nucleic acid delivery and other biomedical applications, Biomacromolecules 19 (9) (2018) 3861–3873.
[29] E. Song, et al., Surface chemistry governs cellular tropism of nanoparticles in the brain, Nat. Commun. 8 (15322) (2017) 15322.
[30] L. Christensen, et al., Solid-phase synthesis of peptide nucleic acids, J. Pept. Sci. 1 (3) (1995) 175–183.
[31] Y. Deng, et al., The effect of hyperbranched polyglycerol coatings on drug delivery using degradable polymer nanoparticles, Biomaterials 35 (24) (2014) 6595–6602.
[32] P.L. Sulkowski, et al., 2-Hydroxyglutarate produced by neomorphic IDH mutations suppresses homologous recombination and induces PARP inhibitor sensitivity, Sci. Transl. Med. 9 (375) (2017) eaal2463.
[33] S. Wagner, et al., Uptake mechanism of ApoE-modified nanoparticles on brain capillary endothelial cells as a blood-brain barrier model, PLoS One 7 (3) (2012) e32568.
[34] A.R. Neves, et al., Apo E-functionalization of solid lipid nanoparticles enhances brain drug delivery: uptake mechanism and transport pathways, Bioconjug. Chem. 28 (4) (2017) 995–1004.
[35] R. Dal Magro, et al., ApoE-modified solid lipid nanoparticles: a feasible strategy to cross the blood-brain barrier, J. Contr. Release 249 (2017) 103–110.
[36] J. Li, et al., < em > PTEN < /em > , a Putative protein tyrosine Phosphatase gene Mutated in human brain, breast, and Prostate cancer, Science 275 (5308) (1997) 1943–1947.
[37] [cited 2018 November 5]; Available from: clinicaltrials.gov..
[38] J. Cui, et al., Ex vivo pretreatment of human vessels with siRNA nanoparticles provides protein silencing in endothelial cells, Nat. Commun. 8 (1) (2017) 191.
[39] H. Lv, et al., Toxicity of cationic lipids and cationic polymers in gene delivery, J. Contr. Release 114 (1) (2006) 100–109.
[40] K.B. Knudsen, et al., In vivo toxicity of cationic micelles and liposomes, Nanomed. Nanotechnol. Biol. Med. 11 (2) (2015) 467–477.
[41] Koul, D., PTEN Signaling Pathways in Glioblastoma. (1555-8576 (Electronic)).
[42] S.T.S. WONG, et al., MicroRNA-21 inhibition enhances in vitro chemosensitivity of temozolomide-resistant glioblastoma cells, Anticancer Res. 32 (7) (2012) 2835–2841.
[43] J. Kreuter, et al., Covalent attachment of apolipoprotein A-I and apolipoprotein B-100 to albumin nanoparticles enables drug transport into the brain, J. Contr. Release 118 (1) (2007) 54–58.
[44] J.K. Saucier-Sawyer, et al., Distribution of polymer nanoparticles by convection-enhanced delivery to brain tumors, J. Contr. Release 232 (2016) 103–112.